# Vertical grid refinement for stratocumulus clouds in the radiation scheme of a global climate model

Paolo Pelucchi[1,2], David Neubauer[1], and Ulrike Lohmann[1]

[1]Institute of Atmospheric and Climate Science, ETH Zurich, Zurich, Switzerland
[2]Now at Universitat de València, Valencia, Spain

**Correspondence:** Paolo Pelucchi (paolo.pelucchi@uv.es), David Neubauer (david.neubauer@env.ethz.ch)

**Abstract.** In this study, we implement a vertical grid refinement scheme in the radiation routine of the global aerosol-climate model ECHAM-HAM, aiming to improve the representation of stratocumulus clouds and address the underestimation of their cloud cover. The scheme is based on a reconstruction of the temperature inversion as a physical constraint for the cloud top. On the refined grid, the boundary layer and the free troposphere are separated and the cloud's layer is made thinner. The cloud

5 cover is re-calculated either by conserving the cloud volume (SC-VOLUME) or by using the Sundqvist cloud cover routine on the new grid representation (SC-SUND). In global climate simulations, we find that the SC-VOLUME approach is inadequate, as in most cases there is a mismatch between the layer of the inversion and of the stratocumulus cloud, which prevents its application and is itself likely caused by too-low vertical resolution. With the SC-SUND approach, the possibility for new clouds to be formed on the refined grid results in a large increase in mean total cloud cover in stratocumulus regions. In both

10 cases, however, the changes exerted in the radiation routine are too weak to produce a significant improvement of the simulated stratocumulus cloud cover. The grid refinement scheme could be used more effectively for this purpose if implemented directly in the model's cloud microphysics and cloud cover routines.

## 1 Introduction

Stratocumulus (Sc) clouds belong to the low-level stratiform clouds. They occur in many regions and cover large areas of the

15 Earth's surface, but appear most frequently over the oceans. In particular, the subtropical eastern Pacific and Atlantic oceans, west of the continental land masses of North America, South America and southern Africa, experience stratocumulus clouds in excess of 40% of the time (Wood, 2012), in what are referred to as the semi-permanent subtropical marine stratocumulus sheets. Stratocumulus clouds are of considerable importance to the Earth's radiative budget, as they exert a very strong net negative cloud radiative effect. This is due to a combination of a weak longwave effect due to their low-lying position on the

20 one hand, and of an especially strong reflection of shortwave solar radiation accentuated by their location over dark oceans on the other.

Despite the crucial role of stratocumulus clouds for the climate, their representation in global climate models (GCMs) still has major deficiencies (Boucher et al., 2013). Cloud cover in stratocumulus regions tends to be underestimated (Nam et al., 2012; Neubauer et al., 2014). The representation of stratocumulus clouds is especially challenging due in part to the GCMs'

25 relatively coarse vertical resolution, which degrades the performance of the parametrisations of related processes such as turbulence, convection, microphysics and vertical advection (Yamaguchi et al., 2017). Low vertical resolution can also be the cause of numerical artefacts such as numerical entrainment (Lenderink and Holtslag, 2000) or spurious radiative-dynamical interactions (Stevens et al., 1999). On a basic level, model gridboxes at the typical level of stratocumulus clouds are generally too thick (a few hundred meters) to resolve the clouds' vertical extent, which can be lower than a hundred meters (Wood,

30 2012). The resulting overestimation of their vertical extent is associated with an underestimation of their horizontal extent. The models' coarse vertical grid is also not adequate to resolve the temperature profile under which stratocumulus clouds form, which is characterised by a sharp inversion. Stratocumulus clouds are generally found just below the top of inversion-capped marine boundary layers. The temperature inversion is an essential feature as it suppresses upwelling motion, limiting convection to within the boundary layer and forcing stratocumulus clouds to spread and develop into extended thin sheets. The

35 inversion can be very sharp, attaining a temperature difference of tens of Kelvin in just a few meters vertically (Roach et al., 1982), and as such provides a net separation between the free troposphere and the stratocumulus-topped boundary layer.

Several studies have approached the problem of poor stratocumulus representation using vertical grid refinement. Grenier and Bretherton (2001) developed a moist planetary boundary layer (PBL) parametrisation for application to subtropical stratocumulus-capped marine boundary layers, which relies on the assumption that the PBL is topped by an infinitely thin inver-

40 sion. They present three methods for reconstructing the inversion pressure. Using the inversion pressure to separate the moist PBL and the free troposphere allows continuous evolution of the cloud depth and cloud top location. Grenier and Bretherton (2001) obtained good results with their scheme and reconstruction in a single column model. However, as they already point out, a scheme with variable grid levels would be difficult to fully implement in a 3D model, where a fixed grid is used for other processes such as horizontal advection. In her PhD thesis, Siegenthaler-Le Drian (2010) applied the diagnostic inversion recon-

45 struction method from Grenier and Bretherton (2001) in the ECHAM-HAM GCM to dynamically refine the vertical resolution in stratocumulus-capped marine boundary layers, adding two new vertical grid levels. However, due to numerical problems, the scheme could not be made fully interactive in the GCM setup. More recently, Yamaguchi et al. (2017) introduced a framework for enhancing the vertical resolution on which certain physical parametrisations are computed with the aim of improving low cloud representation. The method produced significant improvements in simulations of a drizzling stratocumulus-capped PBL,

50 but at the moment still requires further development and testing.

Other approaches have focused on parametrisation of the cloud cover of stratocumulus clouds and on correcting its bias due to low vertical resolution using information about the inversion location. Boutle and Morcrette (2010) presented a scheme which separately calculates the cloud area fraction of stratocumulus clouds (as opposed to the volume fraction usually computed in models) from a subgrid interpolation-extrapolation of the vertical temperature profiles, meant to sharpen and better

55 represent the inversion. This fraction is used only for the radiation scheme, but an improvement in the cloud cover and other fields due to internal feedbacks was also observed. In ECHAM-HAM as well, the cloud cover is calculated as the volume fraction of the gridbox occupied by clouds, and is used as such in the microphysics routine. However the same value is used in the radiation routine as a horizontal area fraction. The underlying assumption reconciling the two interpretations of the model's given cloud cover is that clouds occupy the full vertical extent of a gridbox. This idea results in a misrepresentation of thinner

60  clouds, such as stratocumuli, and their radiative fluxes. Although their in-cloud properties and hence cloud optical depth are correctly estimated, forcing them to occupy the thickness of the model layer results in an underestimation of horizontal extent - of cloud area fraction - which alters the all-sky radiative flux.

In this study, we develop and implement a new simple parametrisation for stratocumulus cloud cover in ECHAM-HAM. We use the inversion reconstruction from Grenier and Bretherton (2001) to define a refinement of the vertical levels in a way

65  that facilitates a more realistic representation of the horizontal extent of simulated stratocumulus clouds. We do not set out to implement the full PBL parametrisation, and instead focus primarily on the stratocumulus cloud cover, using the exact vertical location of the reconstructed inversion as a physical constraint for the cloud top. The number of vertical levels does not increase with our approach as the grid boundary atop the cloudy stratocumulus gridbox is shifted to the inversion pressure, producing a thinner gridbox that matches the true vertical extent of the stratocumulus cloud. In one version of our scheme, we rely on

70  conservation of cloud volume to correct the cloud's horizontal extent, i.e. the cloud cover. In the other, we re-calculate the cloud cover using the cover routine applied on the inversion-based refined grid and profile representations. In order to avoid many numerical problems or difficulties associated with the use of a different grid, we use the new grid and stratocumulus representation only in the radiation scheme of ECHAM-HAM. The radiative effect of stratocumulus clouds is important for climate on a global scale, and hence we hope that the resulting change in radiative transfer and feedbacks can produce an

75  improvement in the simulated stratocumulus clouds overall.

In this article we discuss the implementation and results of our stratocumulus cloud cover parametrisation in ECHAM-HAM. We describe the new scheme's procedure and details of its implementation in Sect. 2 after giving an overview of the model's current treatment of stratocumulus clouds. In Sect. 3.1, we present the results from a test case in single column model (SCM) mode. In Sect. 3.2 and 3.3, we present the results from global climate simulations and discuss the limitations of the scheme's

80  implementation. Finally, we draw our conclusions in Sect. 4.

## 2 Method

### 2.1 Model description

The work is carried out with the global aerosol-climate model ECHAM-HAM, composed of the general circulation model ECHAM and the aerosol microphysics module HAM, in its version ECHAM(v6.3.0)-HAM(v2.3)-P3. This refers to the latest

85  standard release of ECHAM-HAM (Tegen et al., 2019) used with the P3 microphysics scheme developed by Dietlicher et al. (2018). The horizontal resolution is T63 ($1.875° \times 1.875°$) and the vertical is L47 (47 hybrid sigma-pressure levels). The timestep is 450 s and the radiation routine is ran at 'radiation timesteps' i.e. every 7200 s.

For clouds, ECHAM-HAM-P3 uses a two-moment cloud microphysics scheme with one category for cloud droplets and one for ice, and diagnostic parametrisations for rain. Water vapour, liquid and ice are prognostic variables and the cloud cover

90  is diagnosed. ECHAM-HAM's cloud cover scheme is based on the formulation by Sundqvist et al. (1989). Since absolute humidity in the atmosphere varies on scales smaller than the model's gridboxes, subgrid-scale variations in relative humidity (RH) must be parametrised, in order to achieve the formation of clouds in part of the gridbox. The fraction of a gridbox
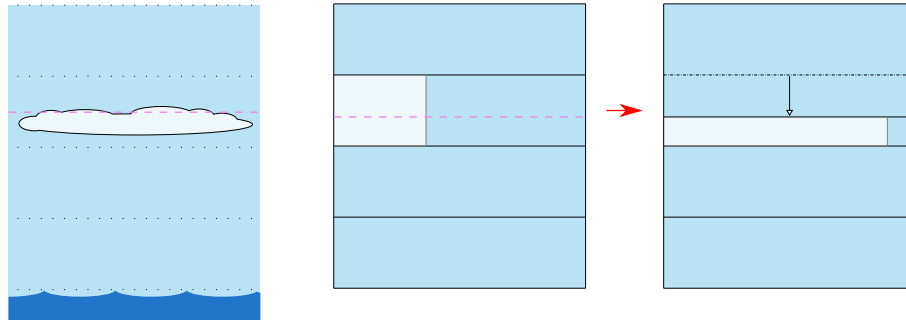
**Figure 1.** Schematic illustrating the idea behind the new stratocumulus representation method. The pink dashed line represents the temperature inversion. On the left is a depiction of the real situation, in the middle its representation in the model's vertical grid, and on the right the same situation on the proposed new vertical grid.

occupied by clouds is named the fractional cloud cover ($clc$). Given the assumed presence of subgrid variations, clouds must start to form when the gridbox mean RH crosses a threshold value $RH_c$ smaller than the saturation relative humidity, $RH_s = 1$. When the threshold is exceeded, the fractional cloud cover is diagnosed according to Sundqvist et al. (1989):

$$clc = 1 - \sqrt{1 - \frac{RH - RH_c}{RH_s - RH_c}} \ . \tag{1}$$

Under low-level inversions, the formula uses adapted parameters (lower $RH_c$ and $RH_s$) with the aim to facilitate the formation of stratocumulus clouds (Mauritsen et al., 2019).

### 2.2 Scheme description

Because the temperature inversion stops vertical motion at the top of the marine boundary layer, we can equate the inversion with the cloud top, and hence use it to constrain the cloud's position and vertical extent. The cloud cover given by the model is the volume fraction that the cloud occupies in the layer. By conserving the cloud volume and restricting the cloud to be found only below the inversion, we reduce its vertical extent and hence increase the horizontal cloud cover, resulting in a more realistic representation of the stratocumulus clouds. The idea is illustrated with a schematic in Fig. 1. This new grid refinement scheme is called *invgrid*. In the following, we will indicate full-levels (model layers or gridboxes) with an integer index and half-levels (grid boundaries) with half-integers, increasing in the downward direction.

An outline of the method is as follows. First, model columns in which a stratocumulus cloud may be present are identified, and the gridbox layer within which the inversion would be found, named the ambiguous layer, is selected. The exact location (pressure level) of the inversion is diagnosed using the 'reconstructed inversion' method described by Grenier and Bretherton (2001), which assumes a certain sub-grid shape of the temperature profile. The inversion is modelled as a discontinuity in the profile, so that it has a single exact pressure value, usable as the cloud top. Once the inversion pressure is known, the overlying model half-level (representing the cloud top) is shifted down to it, resulting in a thinner lower layer in which the stratocumulus cloud is contained, and a larger but cloud-free above-cloud layer of free tropospheric air. The values of the relevant physical

quantities are finally recalculated on this new grid. The new grid boundaries and recalculated quantities are passed to the
115 radiation routine, and the procedure is repeated at every radiation timestep.

The following sections describe the steps in detail, from the detection of applicable columns to the recalculation of all new-grid quantities. The method to calculate the inversion pressure, described in Sect. 2.2.2, follows closely the 'reconstructed inversion' method developed and described by Grenier and Bretherton (2001). The code to calculate the inversion pressure following this procedure was written by Siegenthaler-Le Drian (2010) for her PhD thesis and hence already available in ECHAM-HAM.
120 A few changes implemented during this study are described.

### 2.2.1 Ambiguous layer selection

The criterion used to select columns in which to apply *invgrid* at each timestep is based on low tropospheric stability (LTS). LTS is a measure defined as the difference in potential temperature between the 700 hPa level and the surface. A strong correlation between LTS and low stratiform cloud cover has been found in observations, especially in the subtropics, as shown
125 by e.g. Klein and Hartmann (1993); Wood and Hartmann (2006). A high LTS is attributable to a strong inversion. Based on the climatology of low stratus cover in Klein and Hartmann (1993), a threshold value of 20 K of LTS is used to select the columns with possible stratocumulus clouds, in which to apply the *invgrid* scheme. This criterion was previously used by Siegenthaler-Le Drian (2010) to select columns in which to activate her stratocumulus-entrainment parametrisation. As a possible alternative, the threshold could also be based on the estimated inversion strength (EIS), which, as a more refined
130 measure of inversion strength compared to LTS, may be more robust as a predictor of low stratocumulus cloud cover. This is also because, as pointed out by Wood and Bretherton (2006), the relationship between LTS and cloud fraction is not proven to hold in a warming climate, while the link between EIS and stratocumulus cloud cover is more direct. In the context of this study, the choice of criterion between LTS or EIS is not expected to produce significant differences in the selection of stratocumulus columns, and hence the simpler option is used.
135 In each identified column, the layer in which to look for and reconstruct the inversion must be selected. It is called the "ambiguous layer" by Grenier and Bretherton (2001) because while in reality it would exhibit a lower cloudy part of boundary layer air and an upper cloud-free part of free-tropospheric air, within one model gridbox this vertical distinction cannot be resolved. Finding the inversion pressure allows to separate the two parts. To select the ambiguous layer, we first look for the inversion in the model, i.e. the maximum gradient of temperature. This will be found across two grid layers, which may both
140 potentially contain the inversion jump in a sub-grid profile reconstruction. We choose the ambiguous layer as the uppermost of the two possible layer which contains a cloud, defined as non-zero cloud cover and liquid water content (as in the absence of either of these a cloudy radiative flux is not computed in the model). This selection criterion finds the top of the simulated cloud and hence guarantees that the cloud-rescaling idea would be applicable. If no cloud is present in either of the two possible layers, we use the condition previously used by Siegenthaler-Le Drian (2010): we look at the saturation of an air parcel in an
145 adiabatic ascent from two layers below the inversion, and we choose the ambiguous layer as the layer under the first half-level at which the parcel reaches supersaturation, as it presents the conditions to contain a cloud. This condition operates under the assumption that the stratocumulus is contained within only one layer, as the cloud top could still be found in the layer above.
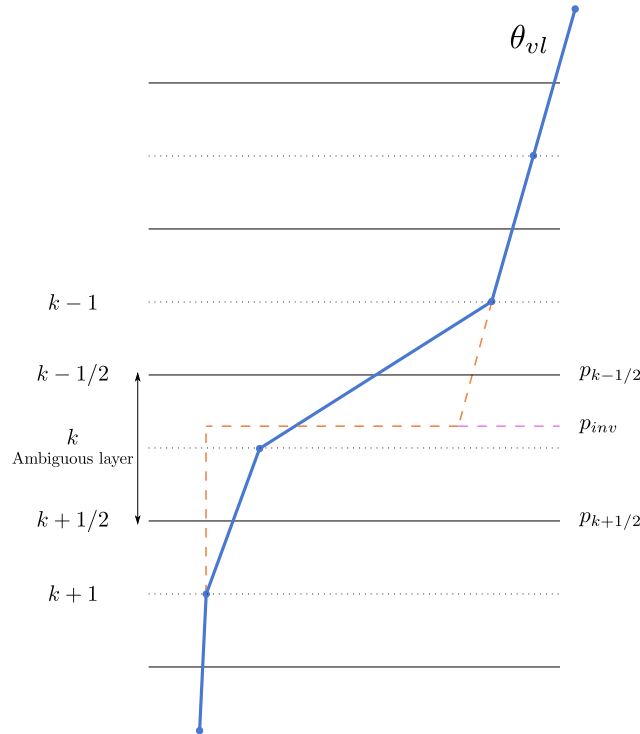
**Figure 2.** Illustration of a $\theta_{vl}$ profile (blue line) and its sub-grid reconstruction (dashed orange line) in the ambiguous layer. The solid and dotted horizontal black lines are the model half-levels and full-levels respectively. The dashed lines extending from levels $k+1$ and $k-1$ represent the assumed sub-grid $\theta_{vl}$ profile within the ambiguous layer, and are obtained as described in Sect. 2.2.2. The discontinuity in the sub-grid profile constitutes the inversion pressure $p_{inv}$.

The scheme allows the possibility to re-attempt the inversion reconstruction calculation one layer above if it fails in the first selected ambiguous layer.

### 2.2.2 Inversion reconstruction

We diagnose the inversion pressure following the method developed and described by Grenier and Bretherton (2001); the procedure is repeated here for convenience of the reader and to indicate our modifications.

The inversion pressure reconstruction method by Grenier and Bretherton (2001) is based on reconstructing the sub-grid profile of virtual liquid water potential temperature ($\theta_{vl}$) in the ambiguous layer $k$, in which its value $\theta_{vl}^k$ is considered the weighted average of its below-inversion (boundary layer) and above-inversion (free-tropospheric) values. Figure 2 shows a diagram of an example profile, with labelled layer indices.

The virtual liquid water potential temperature is defined as

$$\theta_{vl} = T \left( \frac{p_0}{p} \right)^{\frac{R_d}{c_{pd}}} \left( 1 - \frac{L_v}{c_{pd}T} q_l \right) \left( 1 + \left( \frac{R_v}{R_d} - 1 \right) q_t \right), \tag{2}$$

where $T$ is temperature, $p$ is pressure ($p_0 = 1000$ hPa), $R_d$ and $R_v$ are the dry air and water vapour gas constants, $L_v$ is
the latent heat of vaporisation, $q_l$ and $q_t$ are the liquid and total water contents (mass mixing ratios), and $c_{pd}$ is the constant
pressure heat capacity of air. $\theta_{vl}$ depends linearly on temperature, and hence exhibits the same vertical profile features (notably
the inversion), with the advantage of being a conserved quantity in a reversible moist adiabatic process, i.e. a process where all
the condensate remains within the air parcel. The inclusion of the 'potential' and 'liquid water' part (second and third factors
on the right hand side of the equation) causes the quantity to be conserved, while the 'virtual' part (fourth factor) allows to use
the dry-air equation of state. This makes the quantity advantageous to use in calculations, and hence $\theta_{vl}$ is used for the profile
reconstruction.

On a sub-grid scale, within the ambiguous layer, we distinguish between an above-inversion and a below-inversion profile,
and assume that $\theta_{vl}$ follows

$$\theta_{vl}(p) = \begin{cases} \theta_{vl}^{k+1}, & p_{k+1/2} > p > p_{inv} \\ \theta_{vl}^{k-1/2} + s\left(p - p_{k-1/2}\right), & p_{inv} > p > p_{k-1/2} \end{cases} . \tag{3}$$

Below the inversion, $\theta_{vl}$ has the same value that it does lower down in level $k+1$, justified by the fact that in the case of a
strong inversion, the boundary layer tends to be very well-mixed, in which case $\theta_{vl}$ is constant throughout the well-mixed layer.
Above the inversion, the $\theta_{vl}$ profile is extrapolated down from the overlying level, using the maximum negative gradient with
respect to pressure ($s$) chosen from the gradients across half-levels $k-1/2$ or $k-3/2$.

This profile implies that at the inversion pressure $p_{inv}$, $\theta_{vl}$ experiences a discontinuity, where the value jumps from the
boundary layer to the free troposphere one, representing the sharp inversion. The inversion pressure is found by requiring
conservation of $\theta_{vl}$ within the ambiguous layer, i.e. by requiring that the integral of the sub-grid profile is equal to the original
value of $\theta_{vl}$ in the ambiguous layer $k$ ($\theta_{vl}^k$, considered to be the gridbox average):

$$\theta_{vl}^k = \frac{1}{p_{k+1/2} - p_{k-1/2}} \int_{p_{k-1/2}}^{p_{k+1/2}} \theta_{vl}(p)\, dp \tag{4}$$

$$= \frac{1}{p_{k+1/2} - p_{k-1/2}} \left( \int_{p_{k-1/2}}^{p_{inv}} \theta_{vl}^{k-1/2} + s\left(p - p_{k-1/2}\right) dp + \int_{p_{inv}}^{p_{k+1/2}} \theta_{vl}^{k+1} dp \right) \tag{5}$$

In order to solve Eq. (5) for the inversion pressure, we define the above-inversion mass fraction of the ambiguous layer,

$$\mu = \frac{p_{inv} - p_{k-1/2}}{p_{k+1/2} - p_{k-1/2}} . \tag{6}$$

Equation (5) can then be turned into a quadratic equation in $\mu$:

$$\frac{1}{2} s \left(p_{k-1/2} - p_{k+1/2}\right) \mu^2 - (\theta_{vl}^{k-1/2} - \theta_{vl}^{k+1})\mu + (\theta_{vl}^k - \theta_{vl}^{k+1}) = 0 . \tag{7}$$

The physical solution for $\mu$ is a value between 0 and 1 which, when it exists, can be shown to be the smaller solution of Eq. (7).
If and when a physical $\mu$ is found, the inversion pressure $p_{inv}$ is obtained inversely from Eq. (6). In a following step, $p_{inv}$ is
used to define the new grid.

A limitation of this method is that it requires a well-mixed $\theta_{vl}$ profile in the PBL to successfully obtain the inversion pressure; specifically, the $\theta_{vl}$ gradient with respect to pressure must be negative both below and above the inversion. While this is a characteristic of stable profiles, we noticed that the method sometimes gave inconsistent results when the profiles slightly deviated from being well-mixed. We included a few minor modifications to the method to allow it to be used in more, although less ideal, situations. For example, we force a small but negative $s$ $(-1 \times 10^{-6}\,\mathrm{K\,Pa^{-1}})$ if the gradient above the inversion is only slightly positive (which would normally be considered unusable). We also attempt to carry out the inversion reconstruction in the upper possible ambiguous layer if it fails in the lower one.

### 2.2.3 Grid refinement

As the new representation is used exclusively in the radiation routine, the grid refinement is applied only in cases where it would make a difference to the radiative transfer calculations, specifically by increasing the cloud cover. Hence, we first check that the ambiguous layer contains a cloud, as this is a necessary condition for the radiation routine to compute a cloudy flux. We also ensure that the gridbox layer would not become thinner than a minimum thickness. The limit is put in place to prevent unphysical situations, such as for example a too-high liquid water mixing ratio or cloud droplet concentration. We choose a threshold of $50\,\mathrm{m}$, as stratocumuli are almost never observed to be thinner according to cloud thickness climatologies such as in Wood (2012).

If the conditions are appropriate, we proceed with defining the new refined grid. The half-level above the inversion, the top of the ambiguous layer, is shifted down to the inversion pressure $p_{inv}$. Level $k$ becomes thinner, and will wholly contain the cloud that was originally present in the ambiguous layer. Level $k-1$ on the other hand becomes larger, and will represent the first layer of free tropospheric air.

Once the new grid is defined, the variables that need to be passed to the radiation routine are calculated in the new layers using the assumed sub-grid profile, conservation principles, and the notion that the stratocumulus in the new grid is constrained below the inversion. The procedure for each variable is detailed in the following. Superscripts $k$ and $k-1$ refer to variables and layers in the original model grid, i.e. the ambiguous layer and the overlying layer respectively. We use superscripts $kinv$ for the new thinner layer (equivalent to the below-inversion fraction of the ambiguous layer), $abinv$ for the above-inversion fraction of the ambiguous layer (note that this is not a layer in its own right on either grid), and $kinv-1$ for the new larger overlying layer, consisting of layers $abinv$ and $k-1$.

**Water content reconstruction**

The water vapour $q_v$, liquid water $q_l$ and ice $q_i$ contents are defined as mass mixing ratios $(\mathrm{kg\,kg_{air}^{-1}})$ in the model. The total water content $q_t$ is the sum of all three individual phases and must be conserved.

For consistency with $\theta_{vl}$, we require that $q_t$ follows the same sub-grid profile in the ambiguous layer, and start by calculating it as

$$q_t^{kinv} = q_t^{k+1} \tag{8}$$

$$q_t^{abinv} = \frac{q_t^k - (1-\mu)q_t^{k+1}}{\mu} \tag{9}$$

220   where the second equation is a solution to conservation of $q_t$ in layer $k$, given the above-inversion mass fraction $\mu$ of the ambiguous layer. Its value in $kinv-1$ is obtained as a mass-weighted average of $abinv$ and $k-1$:

$$q_t^{kinv-1} = \frac{q_t^{abinv}M^{abinv} + q_t^{k-1}M^{k-1}}{M^{abinv} + M^{k-1}} \tag{10}$$

where $M$ is the air mass of a layer and the denominator is equal to the air mass in $kinv-1$.

Since liquid water and ice are the components that make up the cloud, we restrict them to be found only below the inversion, 225   in the new thinner cloud layer $kinv$. The total liquid and ice mass is conserved, which means the mixing ratio is simply rescaled to the new layer mass:

$$q_{l/i}^{kinv} = q_{l/i}^k \frac{M^k}{M^{kinv}} \ . \tag{11}$$

The quantities $q_l$ and $q_i$ are thus assumed to be zero in $abinv$, and for layer $kinv-1$ the values in $k-1$ are rescaled to the larger layer. This recalculation does not change the in-cloud values of $q_l$ and $q_i$, which are used in the radiation routine, as the 230   cloud volume is conserved.

The calculation of the water vapour content in the new layers $kinv$ and $kinv-1$ uses the previously calculated reconstructed total water and the inversion-constrained liquid and ice water contents:

$$q_v = q_t - q_l - q_i \ . \tag{12}$$

We recognise that the method for recalculating the water contents described in this section is not fully consistent. In fact, 235   the total water content is treated as a separate variable (as opposed to using the sum of the individual phases of water) and is reconstructed using the sub-grid profile which depends on the under- and overlying layers; at the same time the liquid and ice contents are taken from the ambiguous layer and simply moved to the below-inversion part. This can lead to an inconsistency in the water vapour content especially in the new cloudy layer $kinv$ (in which the air should be saturated), as it is calculated by subtracting the rescaled liquid and ice contents (from layer $k$) from the total $q_t$ (from layer $k+1$). In $kinv-1$ the inconsistency 240   is negligible as there should be no liquid or ice water there. We decided to move forward with this method despite this problem because it has the following advantages. With this method, the liquid and ice contents used for the cloud are the ones that are calculated in the cloud microphysics routine, which takes into account fundamental microphysical processes. Also, the resulting total water below the inversion is equal to the one in the layer below, as is characteristic of well-mixed boundary layers. Overall, the method gives reasonable results for $q_v$ above the inversion and for $q_l$ and $q_i$ in the cloudy layer below it, 245   and the total water content as sum of the individual components is indeed conserved. Checks are in place to prevent and fix potential unphysical (negative) values of $q_v$, $q_l$, $q_i$ or $q_t$.

**Temperature**

The temperature on the new grid is calculated using energy conservation. First, in $kinv$, $T$ is obtained inversely from $\theta_{vl}^{kinv}$ (Eq. (2)). Then, the heat content $H$ of the original layers $k$ and $k-1$ is calculated, along with the heat content of new layer

250 $kinv$:

$$H^j = \left( c_{pd} + c_{pv}q_v^j + c_{lw}q_l^j + c_{iw}q_i^j \right) M^j T^j \tag{13}$$

where superscript $j$ indicates the layer considered and $c_{pv}$, $c_{lw}$ and $c_{iw}$ are the vapour, liquid water and ice specific heat capacities. Then, for energy conservation over the two layers between the original and new grid, $T^{kinv-1}$ is obtained from

$$T^{kinv-1} = \frac{H^k + H^{k-1} - H^{kinv}}{\left( c_{pd} + c_{pv}q^{kinv-1} + c_{lw}q_l^{kinv-1} + c_{iw}q_i^{kinv-1} \right) M^{kinv-1}} \ . \tag{14}$$

255 **Further cloud variables**

Similar to $q_l$ and $q_i$, we confine all cloud variables of the ambiguous layer $k$ to the new thinner layer $kinv$, which is capped by the inversion. The recalculation invokes conservation of cloud volume for cloud cover ($clc$), and particle number for cloud droplet and ice crystal number concentrations ($n_{cd}$, $n_{ic}$). The in-cloud concentrations hence also remain constant. The variables are simply scaled to the new layer thickness $Z$, essentially 'squeezed' under the inversion:

260 $$n_{cd/ic}^{kinv} = n_{cd/ic}^k \frac{Z^k}{Z^{kinv}} \tag{15}$$

$$clc^{kinv} = clc^k \frac{Z^k}{Z^{kinv}} \tag{16}$$

The cloud cover is of course constrained not to exceed $100\%$.

The new half- and full-level pressures (grid boundaries) and all the recalculated new-grid variables are finally passed to the radiation routine.

265 **2.3  Model versions**

The model versions that were used to perform the simulations discussed in the next sections are presented in the following. In addition to the reference model version (REF), two versions implementing *invgrid* were used: one which rescales cloud cover based on cloud volume conservation, as described above, (SC-VOLUME); one which re-calculates the cloud cover on the refined grid by re-running the model's Sundqvist cloud cover scheme (SC-SUND). Another simple scheme (SC-MAX) was

270 used to test and provide an understanding of the potential and limitations of the different *invgrid* versions.

**2.3.1  REF**

The model version ECHAM(v6.3)-HAM(v2.3)-P3 is used as the base model version and referred to as REF (Dietlicher et al., 2018; Tegen et al., 2019). Simulations conducted with REF illustrate the baseline performance of the model and provide the

reference to which simulations conducted with the new schemes developed in this thesis are compared. A brief description of
275  REF and its relevant schemes is given in Sect. 2.1 of this chapter.

### 2.3.2 SC-VOLUME

In the SC-VOLUME model version, the *invgrid* scheme described in Sect. 2.2 is fully implemented in the model. The cal-
culation of the inversion pressure as in Sect. 2.2.2 is performed at every timestep before the radiation routine for diagnostic
reasons. At radiation timesteps, the value is used to refine the vertical grid; physical variables are recalculated as described in
280  Sect. 2.2.3, with the stratocumulus cloud cover calculation being based on cloud volume conservation. These are passed to the
radiation routine.

### 2.3.3 SC-SUND

In the SC-SUND model version, after executing the *invgrid* grid refinement, the stratocumulus cloud cover is calculated by
running the model's Sundqvist cloud cover scheme. The goal is to address cases in which, on the original grid, no cloud is
285  present in the ambiguous layer. This could be due to the ambiguous layer's water vapour mixing ratio being an average between
dry tropospheric air and moist boundary layer air, which may cause the gridbox average relative humidity to be too low to reach
the threshold for forming cloud cover according to Eq. (1). With the new grid's reconstruction, the two different air masses
are separated, which may allow a cloud to form in the new thinner layer, now made up exclusively of boundary layer air and
hence presumably having a higher relative humidity. This would be valuable because it would lead to a better representation
290  of stratocumulus clouds in layers in which the method of SC-VOLUME could not be applied due to the lack of a cloud in the
model in the first place. This method makes use of the refined grid and recalculated profiles of water content and temperature,
but the cloud volume is not necessarily conserved as the cloud cover is recomputed with the cloud cover scheme. The procedure
is only applied if the layer in which a new cloud cover is calculated contains liquid water (or cloud ice). The new cloud cover
representation is only used in the radiation routine.

### 2.3.4 SC-MAX

The SC-MAX model version was designed to investigate the maximum possible effect of a scheme that increases the cloud
cover of existing stratocumuli, such as in SC-VOLUME. This is done by always increasing the cloud cover to 100% in model
layers where a stratocumulus cloud is identified. The cloud cover increase is applied in the same cases in which SC-VOLUME's
cloud rescaling would be, i.e. when the identified ambiguous layer contains a cloud, but also when the ambiguous layer contains
300  no cloud but another layer, at most two levels below it, does. We still consider the latter case as a stratocumulus cloud. The
cloud cover of the first (uppermost) cloudy model layer below the inversion is set to 100%. The modified cloud cover is passed
to the radiation routine.

## 2.4 Experiment description

For each model version, we performed a 15-year-long (2000–2014) global climate simulation with prescribed AMIP sea-surface temperatures (PCMDI, 2018) to evaluate the stratocumulus cloud representation. We used the standard ECHAM-HAM T63/L47 spatial resolution and 450 s (7.5 minute) timestep. The data from the *invgrid* routine is sampled at radiation timesteps, i.e. every 2 hours. As an observational reference for total cloud cover, we used Cloud-Aerosol Lidar and Infrared Pathfinder Satellite Observations (Calipso) data from the GCM-Oriented Calipso Cloud Product (GOCCP) dataset (Chepfer et al., 2010).

## 3 Results and discussion

### 3.1 Single Column Model

We first tested *invgrid*'s inversion reconstruction and grid refinement in ECHAM-HAM's single column model (SCM) mode (Dietlicher et al., 2018). Using the SCM allows us to closely observe the evolution of the vertical profiles and how *invgrid* responds to them. Additionally, the possibility to use observational forcings for the SCM is a method to test the model's representation of real situations and to generally validate the reconstructions of the new scheme. The validation in the SCM was carried out using a forcing derived from observations made during the EPIC campaign (Bretherton et al., 2004), specifically from a segment between 16–22 October 2001 in the southeastern Pacific, where the vertical structure of the boundary layer capped by a persistent stratocumulus cloud was observed using radiosondes and remote sensing (Bretherton, 2005). The EPIC campaign also provided observations of the cloud top and base in this period, obtained with cloud radar and ceilometer respectively (Caldwell et al., 2005), which are used to validate the found inversion heights.

Figure 3 shows the evolution of the cloud top and base over the 6-day period of the EPIC campaign. The cloud top follows the PBL's diurnal cycle, rising during the night due to longwave cloud top cooling driving entrainment and sinking during the day due to absorption of solar radiation suppressing entrainment. The reconstructed inversion generally captures this diurnal cycle. While the exact height of the inversion is at times overestimated (days 1, 4), most of the time it matches the observed cloud top quite well, especially on days 2, 3 and 6. The occasional sudden jumps of the inversion pressure (e.g. between days 1 and 2) occur due to the selection criterion for the ambiguous layer depending on the maximum gradient of $\theta_{vl}$, whose level can change suddenly when the inversion is not very sharp. Finding a criterion which could address this undesirable issue without loss of generality proved difficult. We also calculated the lifting condensation level (LCL) for an air parcel rising from the surface to attempt to estimate the cloud base, but the results exhibited large oscillations and did not match the cloud base most of the time, rendering the LCL diagnostic unsuitable as a proxy for cloud base. A reconstruction of the cloud base would be beneficial to the scheme to complement the constraint of the cloud's extent from above with a constraint from below, resulting in a further improved representation, but the development of a method for accurately diagnosing the cloud base of stratocumulus clouds is outside the scope of this study. In comparison to the inversion reconstruction performed by Siegenthaler-Le Drian (2010), who also tested it in the SCM with the EPIC data, with the modifications added in our method the inversion is found also
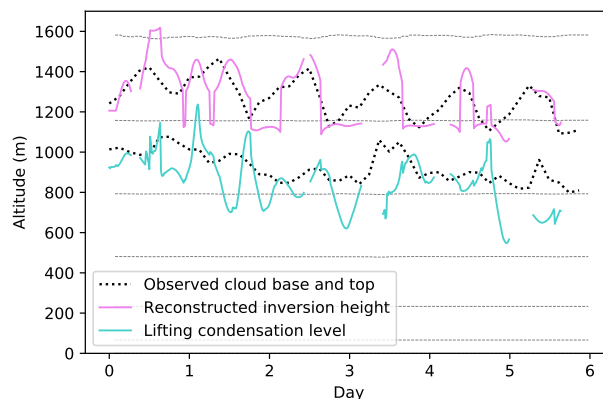
**Figure 3.** Observed cloud base and top during the stratocumulus segment of the EPIC campaign (Bretherton, 2005), and reconstructed inversion and LCL height. The grey dashed horizontal lines are model half-levels in ECHAM-HAM. The time series starts on 15 October 2001, 18:00 local time.
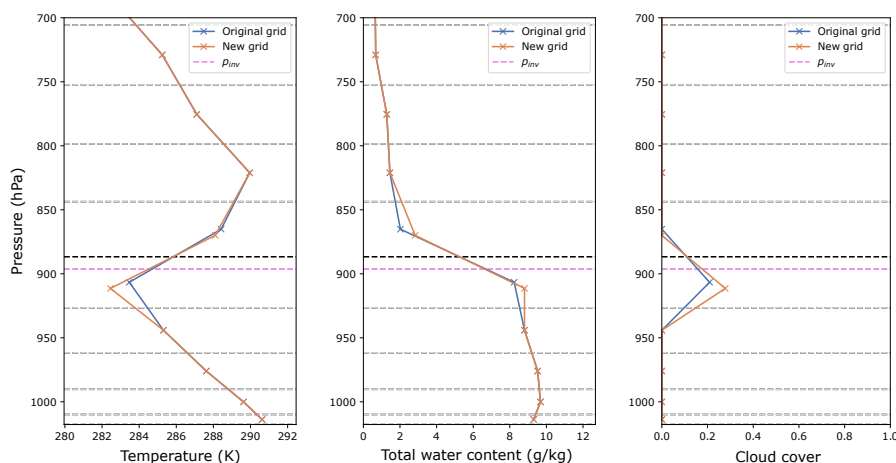
**Figure 4.** Example vertical profiles of the EPIC SCM experiment obtained with the original and new (refined) model grid at the end of day 5 (hour 118). The grey dashed lines represent half-levels common to both grids. The black dashed line represents the top of the ambiguous layer on the original grid; it is shifted to the inversion pressure (magenta dashed line) for the refined grid.

in cases where the method previously failed, for example at the start of the first day or during day 6. Overall, the inversion
335 reconstruction method gives good results for finding the location of the stratocumulus cloud top.

We show some example vertical profiles which occurred during EPIC to illustrate the effect of the grid refinement on temperature, total water mixing ratio and cloud cover in Fig. 4. The inversion in the physical quantities is sharper, and demonstrates the better separation between the PBL and the free troposphere on the refined grid. The cloud cover increases by 6 percentage points - or by almost 30% - as a result of the lower vertical extent of the layer.

340    The EPIC SCM experiment was simulated with the REF, SC-VOLUME and SC-SUND model set-ups; Fig. 5 shows the cloud cover below 800 hPa for each experiment. Only the cloud cover belonging to layers which also have a non-zero liquid water content is shown. In the REF simulation, the cloud is mostly contained within one layer in the model. In fact, it is found most often in the layer below the one containing the inversion, and hence in which cloud top was predicted (and observed) to be. In these situations, with SC-VOLUME the cloud rescaling cannot be applied, as the layer containing the inversion

345    contains no cloud, and hence the reconstruction would not make a difference to the radiation routine. The three times where the model's cloud extends into the upper layer, the *invgrid* scheme is applied effectively, reducing the thickness of the top cloudy layer following the inversion and hence obtaining a more realistic depiction. The SC-SUND scheme version was developed in response to the issue described above: it uses a better water profile representation by applying the refined grid also in the cloud cover routine, so that possibly a new cloud can be formed right below the inversion that is missing when using the original grid.

350    In the SC-SUND simulation, a new cloud is formed in a few cases in the upper layer (days 1, 2, 4) and once in the central layer at the end of day 5. The scheme actually simulates a new cloud cover more frequently, but the lack of water condensate in the inversion layer limits the number of 'valid' instances. A more ideal representation of the water content in addition to $clc$ would be obtained if the grid refinement method were used in the microphysics routines too. Such an implementation comes with the aforementioned challenges that our more limited usage of the new scheme in the radiation routine only aimed to avoid.

355    In our analysis of the global simulations we also investigate the frequency of situations such as those observed in the EPIC simulations, in which the model's simulated cloud is in the layer below where we expect to find it via the inversion reconstruction.

### 3.2    Global Climate Simulations

After demonstrating the desired functioning of *invgrid* in the SCM, we studied its effect on the stratocumulus cloud cover in

360    global climate simulations. We focus on three subtropical stratocumulus regions, which are known to exhibit semi-permanent marine stratocumulus sheets, namely the oceans just west of North America (NAM), South America (SAM) and southern Africa (AFR). We also look at an Arctic region, over the Barents sea (BAR). The regional averages cited in the text are defined over the areas highlighted in Fig. 6a.

    The reference model version REF generally underestimates cloud cover in the subtropical stratocumulus regions, as shown

365    in Fig. 6b in a comparison to the Calipso-GOCCP satellite climatology (Chepfer et al., 2010). The cloud cover difference exhibits a similar pattern in all three regions: compared to observations, cloud cover is actually overestimated along the coast, such that the overall underestimation results from large areas of lower cloud cover further offshore. In the Arctic, total cloud cover is instead overestimated by the model.

    The results from the simulations with the modified schemes are shown in Fig. 6c-h, with on the right hand side the annual

370    mean simulated total cloud cover, and on the left hand side the total cloud cover change experienced by the radiation routine, i.e. the difference between after and before the application of the *invgrid* scheme. The total cloud cover in the simulations can change when changes by the invgrid scheme on cloud radiative effects feed back on the clouds, e.g. by increased turbulence through stronger cloud top cooling. Regional averages are reported in Table 1.
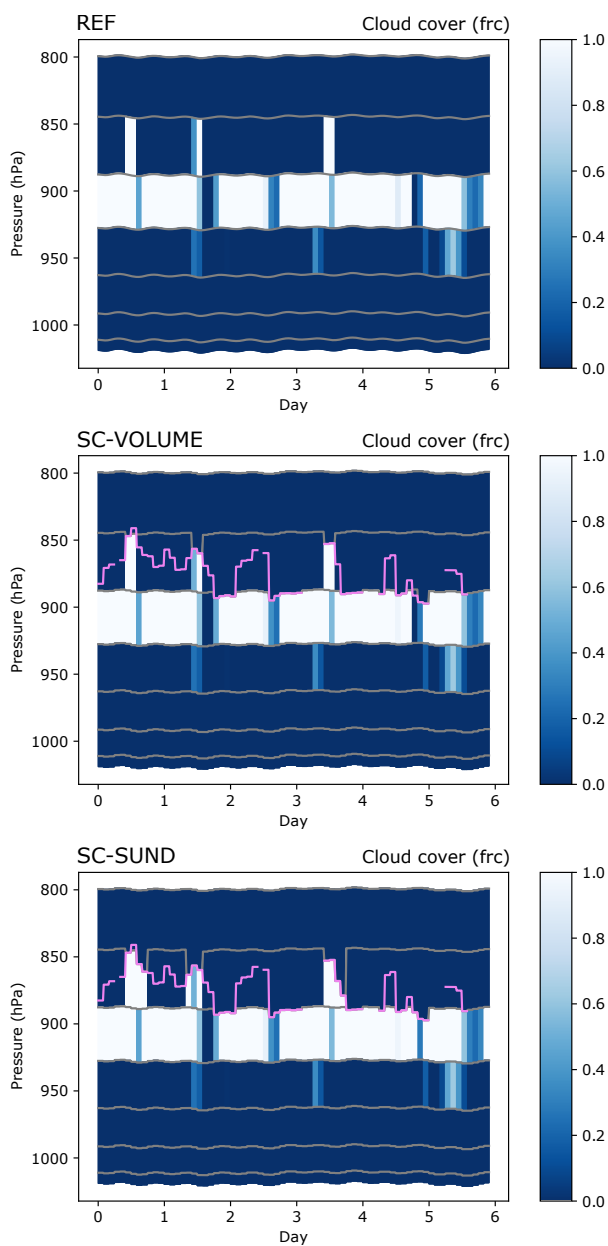
**Figure 5.** Cloud cover fraction of clouds in the EPIC SCM simulations in REF, SC-VOLUME and SC-SUND. The grey lines represent the model half-levels, the magenta line is the reconstructed inversion pressure. The inversion's evolution in time appears more step-like than in Fig. 3 because the refined grid is only applied for the radiation routine at radiation timesteps (every 7200 s).
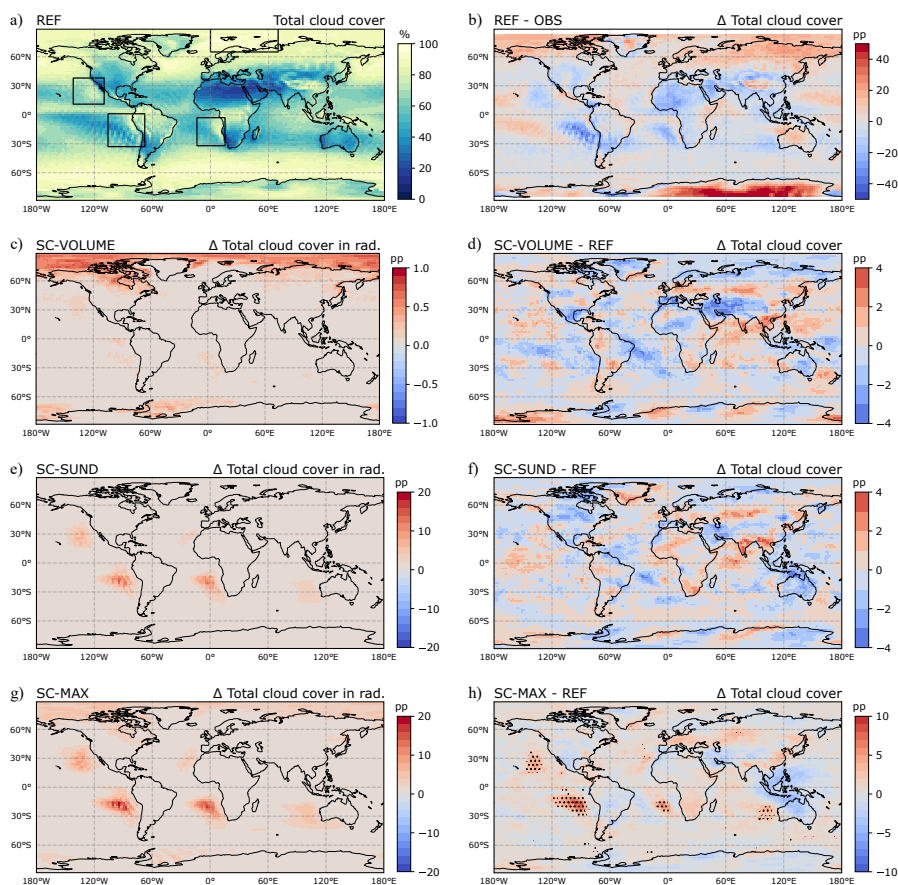
**Figure 6.** Total cloud cover results from 15-year free global climate simulations. Reference results (REF): (a) total cloud cover, (b) difference with Calipso climatology. Results with SC-VOLUME, SC-SUND, SC-MAX: (c)–(h) on the left, total cloud cover increase exerted in the radiation routine; on the right, change in simulated total cloud cover compared to REF (stippling indicates statistically significant differences at the 95% significance level; the false discovery rate is controlled following Wilks (2017)).

The regions highlighted in Fig. 6a are defined as follows: NAM: 38°N–11°N, 142°W–110°W; SAM: 1°N–33°S, 106°W–68°W; AFR: 3°S–32°S, 14°W–15°E; BAR: 90°N–65°N, 0°E–70°E.

In the SC-VOLUME simulation, the increase in total cloud cover caused by *invgrid* and seen by radiation in the annual mean is extremely small in stratocumulus regions, reaching at most 1 percentage point (pp) in the Arctic where it is most marked. As the changes in the radiation routine are small, the change induced to the simulated cloud cover due to internal climate feedbacks is also very small. A simple two-sided t-test using the annual means showed that the results do not differ from REF in a statistically significant manner; they also do not exhibit an explicable pattern (Fig. 6d). The changes in cloud radiative effects produced with SC-VOLUME were much weaker than we had initially expected (not shown), and in Sect. 3.3 we investigate the factors that limit the effectiveness of the SC-VOLUME method in global simulations.

**Table 1.** Annual mean total cloud cover and differences between simulations, as global and regional averages. An asterisk denotes statistically significant differences at the 95% significance level. "Δ seen by rad. " indicates the change in total cloud cover produced with *invgrid*, which is then applied only in the radiation routine.

| Total cloud cover | Global | NAM | SAM | AFR | BAR |
|---|---|---|---|---|---|
| Calipso (%) | 67.2 | 69.1 | 71.7 | 66.5 | 82.6 |
| REF (%) | 66.4 | 63.0 | 58.3 | 58.2 | 89.6 |
| REF minus Calipso (pp) | -0.9 | -6.0 | -13.5 | -8.4 | +7.0 |
| SC-VOLUME minus REF (pp) | -0.12 | -0.39 | -0.60* | -0.48 | -0.70* |
| SC-VOLUME Δ seen by rad. (pp) | +0.04 | +0.05 | +0.06 | +0.06 | +0.18 |
| SC-SUND minus REF (pp) | -0.10 | +0.12 | +0.08 | 0.00 | -0.46 |
| SC-SUND Δ seen by rad. (pp) | +0.57 | +2.13 | +3.01 | +3.63 | +0.47 |
| SC-MAX minus REF (pp) | +0.26* | +1.44* | +1.72* | +1.36* | +0.01 |
| SC-MAX Δ seen by rad. (pp) | +0.99 | +3.23 | +4.37 | +5.19 | +1.29 |

In the SC-SUND simulation, the possibility to form new clouds on the refined grid gives the potential to produce a larger mean cloud cover increase than with SC-VOLUME. This is in fact the case in the radiation routine (Fig. 6e): as intended, the subtropical stratocumulus regions exhibit large increases (up to 15 pp) in the annual mean total cloud cover. The most affected areas are located away from the continental coasts, i.e. in the regions where ECHAM-HAM most underestimates cloud cover, showing that SC-SUND can accurately address the problem. As for the change induced in the simulated total cloud cover (Fig. 6f), the difference to REF is also small (on the same order of magnitude as with SC-VOLUME), although the spatial patterns seem to indicate a slight reduction of the model bias in subtropical stratocumulus regions. The stronger cloud top radiative cooling could favour convection bringing moisture into the cloud from the surface, increasing stratocumulus cloud longevity in a positive feedback loop affecting the simulated cloud cover. However, the difference with REF was found to be not statistically significant with SC-SUND as well.

With both set-ups, the change exterted is too small to cause significant changes in the simulated total cloud cover. At the same time, the results indicate that, in terms of the initial changes produced in the radiation routine, SC-SUND is more effective than SC-VOLUME at increasing cloud cover in the annual mean. This suggests that the model's bias is less due to an underestimation of cloud extent in individual instances, which SC-VOLUME is designed to address, and more to a negative bias in the frequency of stratocumulus cloud formation, which can be addressed by SC-SUND due to its re-evaluation of cloud cover on the refined grid. Other factors hindering the suitability of SC-VOLUME could also be at play, and they are considered in the following Section.

### 3.3 Further analysis and scheme limitations

#### 3.3.1 Scheme usage frequency in SC-VOLUME

400 For SC-VOLUME's cloud cover reconstruction to produce a significant effect in global simulations, it must be applied frequently in practice. The *invgrid* scheme requires a series of conditions to be met in order to be applied and rescale the ambiguous layer's cloud cover. The occurrence frequency of these conditions in the SC-VOLUME simulation is reported in Table 2.

First of all, the scheme must find and successfully reconstruct a temperature inversion. The associated conditions and calcu-
405 lations, described in Sections 2.2.1 and 2.2.2, result in the inversion being found very frequently in the stratocumulus regions, upwards of 70% in some columns (Figure 7a). In most of these cases, a stratocumulus cloud, defined as a cloudy layer at or below the inversion, is also present (Figure 7b). The occurrence frequency of these identified stratocumulus clouds is lower than in reality, where it is around 46% annually in the relevant regions according to the ship-based observational climatology (1954–1997) by Hahn and Warren (2007). This represents a deficiency of the model and a limitation to the SC-VOLUME
410 scheme's aptness to correct the cloud cover bias. The practical applicability of SC-VOLUME's cloud reconstruction method is even more starkly reduced by the subsequent necessary condition, that the cloud (or at least its upper part) must be found in the same model layer as the inversion. As indicated in Sect. 3.1 and quantified in Fig. 7c, this condition is in fact very rare and occurs in much more limited areas than those in which stratocumulus clouds are identified, concentrated in close proximity of the coasts. Figure 7d shows the conditional probability of the stratocumulus cloud being found in the ambiguous layer, given
415 that a cloud is present below the inversion. This probability decreases with the distance from the coast in the subtropical marine stratocumulus regions, where overall it is less than 25%. The rest of the time, the cloud is at a lower level than the inversion. The conditional probability is instead very high in higher latitudes. This is likely the result of the different meteorological conditions - due to lower temperatures and the presence of ice, the model's RH requirement for cloud cover formation is lower and easier to reach. In addition, the PBL is typically shallower in the Arctic, and as the model's vertical resolution is higher
420 closer to the surface, its vertical structure is better resolved and can more easily form clouds at the right level.

The results indicate that there is a prevalent mismatch between the layer where the inversion is found, which is where the cloud top is expected to be, and where the model in fact forms the cloud, in the layer below the inversion. In these cases, the idea of 'squeezing' the existing cloud under the inversion cannot be used, and hence this discrepancy between predicted and effective location of the cloud in the model greatly reduces the applicability of SC-VOLUME's method, especially in the
425 subtropics.

As the SC-SUND simulations in Sect. 3.2 indicate, the origin of the discrepancy may lie in the nature of the ambiguous layer itself. As it is located across the inversion, variables such as temperature and water vapour concentration would in reality be very different between the bottom and the top of the layer. The ambiguous layer's values hence represent an average of the cold and possibly moist PBL air at the bottom and dry and warm free-tropospheric air at the top. Then, depending on the proportion
430 of boundary layer versus free tropospheric air (i.e. depending on where the inversion lies within the layer), the gridbox mean saturation may or may not be sufficient to form a cloud (see Sect. 2.1). Cloud formation is favoured in high RH conditions of
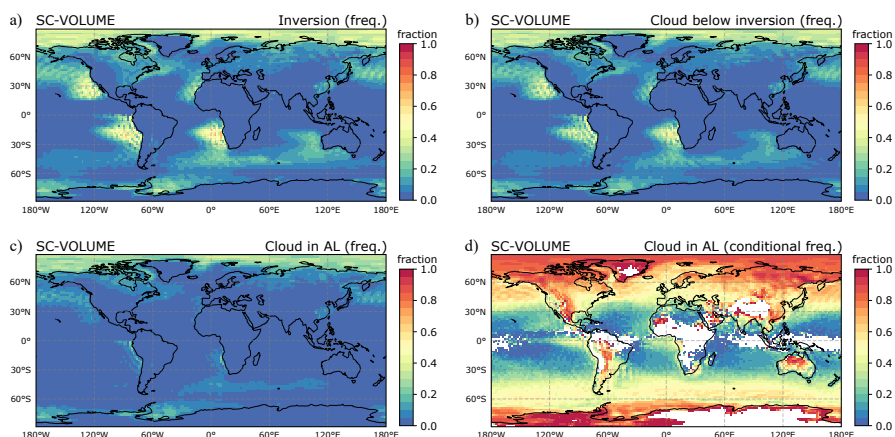
**Figure 7.** Frequency of occurrence of various conditions related to *invgrid* in the SC-VOLUME simulation: (a) an inversion is found, (b) a cloud is present below the inversion, (c) a cloud is present in the ambiguous layer, (d) given that there is a cloud below the inversion, the cloud is in the ambiguous layer (conditional).

**Table 2.** Global and regional average occurrence frequency in the SC-VOLUME simulation of finding an inversion, finding an inversion with an underlying cloud (identified stratocumulus clouds), finding a cloud in the ambiguous layer (AL); and the conditional occurrence frequency of a cloud in the ambiguous layer, given that a cloud is present below the inversion. Also included for comparison are the average frequency of occurrence of stratocumulus clouds from the Hahn and Warren (2007) surface-based observational cloud climatology, averaged over the stratocumulus regions defined in this study.

|  | Global | NAM | SAM | AFR | BAR |
|---|---|---|---|---|---|
| Inversion found (%) | 6.7 | 20.9 | 21.5 | 26.6 | 16.1 |
| Identified Sc cloud (%) | 5.6 | 17.3 | 16.5 | 20.8 | 14.9 |
| Cloud in AL (%) | 2.5 | 4.0 | 3.5 | 4.0 | 11.1 |
| Conditional cloud in AL (%) | 37.4 | 23.6 | 24.0 | 20.9 | 69.8 |
|  | Global (oceans only) | | Stratocumulus regions | | |
| Obs. Sc occurrence frequency (%) | 31 | | 46 | | |
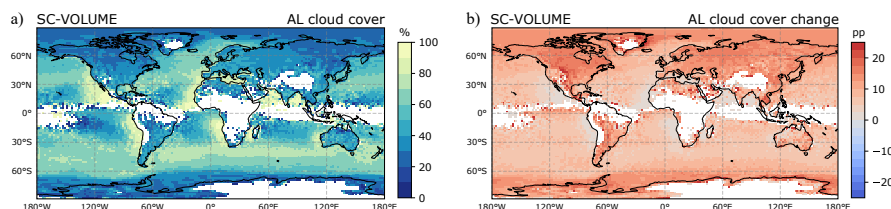
**Figure 8.** Mean (a) cloud cover and (b) cloud cover change in the ambiguous layer with SC-VOLUME, conditionally sampling cases in which the ambiguous layer contained a cloud.

the PBL air, and therefore will be unlikely in the ambiguous layer especially when the inversion is close to its bottom. The layer below the ambiguous layer, being fully located inside the PBL, is instead much more likely to present the conditions appropriate to form a cloud in the model. Thus the stratocumulus cloud is most often found in the layer below the ambiguous

435 layer, rather than in the ambiguous layer itself. The problem we identified of misrepresentation of the cloud's vertical location seems to be a result of poor vertical resolution, just like the underestimation of stratocumulus cloud cover due to exaggeration of their vertical extent. Our scheme aimed to correct the latter, but doing so as we envisioned is difficult without also addressing the former.

### 3.3.2 Maximum cloud cover improvement with SC-VOLUME

440 In addition to only being used in a small fraction of stratocumulus cases, we found that SC-VOLUME's cloud reconstruction does not tend to increase cloud cover very much in the layers in which it is used. Figure 8a shows the mean cloud cover in the ambiguous layer when it contains a cloud. In the stratocumulus regions, close to the coasts the ambiguous layer cloud cover is already very high on average, and hence cannot be increased much further, but farther offshore it decreases as low as 40 %. However, the mean increase produced there is less than 10 pp (Fig. 8b). A probable reason for this is that, when inversion

445 and cloud layer match, the inversion is likely to be high within the layer (as it is the associated higher proportion of PBL in the layer that allowed the formation of a cloud). Hence, the refined layer is not much thinner than the original one, and a volume-conservation-based reconstruction of the cloud cover does not increase it very much. This demonstrates again how the SC-VOLUME method for cloud cover reconstruction is limited by the same biases of the original vertical representation that *invgrid* aims to correct. While the grid refinement can improve the vertical representation, basing the new cloud cover on the

450 flawed original cloud cover gives poor results.

To assess the maximum effect that a scheme such as *invgrid* in SC-VOLUME, increasing the cloud cover for existing stratocumulus clouds, could cause, we performed the SC-MAX experiment. In this simulation, the cloud cover of identified stratocumulus clouds, i.e. the first cloudy layer at or below the inversion level, is set to 100%. The SC-MAX method is applied also to those stratocumulus situations that SC-VOLUME could not affect (in which the cloud and the inversion are not in the

455 same layer). Hence, the SC-MAX method exerts the maximum possible stratocumulus cloud cover increase.

**Table 3.** Global and regional averages of mean ambiguous layer cloud cover ($clc^{kinv}$) and its increase in SC-VOLUME, conditionally sampling cases in which the ambiguous layer contained a cloud.

|  | Global | NAM | SAM | AFR | BAR |
|---|---|---|---|---|---|
| Original $clc^{kinv}$ (%) | 48.7 | 76.3 | 72.4 | 76.5 | 35.4 |
| SC-VOLUME $\Delta clc^{kinv}$ (pp) | +0.5 | +3.7 | +4.4 | +3.4 | +13.6 |

The annual mean total cloud cover difference that is produced for the radiation routine with SC-MAX is very large, as can be seen in Figure 6g. Further, in this case the changes exerted propagate through feedbacks much more evidently, and can be clearly observed in the model's simulated total cloud cover. When comparing it to REF (Fig. 6h), the increase exhibited in the subtropical stratocumulus regions is significant. However, the model's bias compared to observations is still far from being
460   completely corrected, as the average underestimation in the South American region, which experienced the most improvement, is still -11.7 pp with SC-MAX as opposed to -13.5 pp in REF.

The SC-MAX experiment demonstrates that a stratocumulus cloud cover scheme applied only in the radiation routine can have a positive effect on the model via feedbacks, but, in the case of ECHAM-HAM, it is not sufficient to fully close the gap between the simulated and observed cloud cover. Even the cloud cover seen by the radiation routine is still underestimated
465   in the stratocumulus regions compared to the observed climatology. This experiment further confirms that ECHAM-HAM's cloud cover bias is caused also by a lack of stratocumulus clouds in the first place. A scheme affecting only existing clouds, such as in SC-VOLUME, would need to be complemented by improvements in other parametrisation schemes to increase the occurrence of stratocumulus clouds as well.

The SC-SUND scheme presents a possible improvement to this, as it can be applied even in columns with no below-inversion
470   cloud at all, with the possibility to form a new cloud there.

### 3.3.3   New clouds in SC-SUND

The SC-SUND scheme has the potential to address both the issues identified in the previous sections in the SC-VOLUME set-up, namely its inability to address cases in which the stratocumulus is below the inversion layer and the scarcity of simulated stratocumulus in the model.
475   Figure 9a shows the frequency of occurrence of a cloud in the ambiguous layer after SC-SUND's reconstruction, and Fig. 9b its increase compared to the original representation. The SC-SUND scheme forms new clouds up to 30% of the time in the southern marine subtropical stratocumulus regions, also significantly extending over the ocean the area over which the condition occurs. This demonstrates that the separation of PBL and free troposphere achieved with the refined grid is very effective, and allows clouds that could not be formed previously in the coarser gridbox to be 'revealed' on a re-execution of the
480   cloud cover scheme. The overall effect that a newly formed cloud in the ambiguous layer has on total cloud cover depends on the presence of a cloud in other layers: in a previously cloud-free column a new cloud increases the total cloud cover in general more significantly than in a column already containing a cloud.
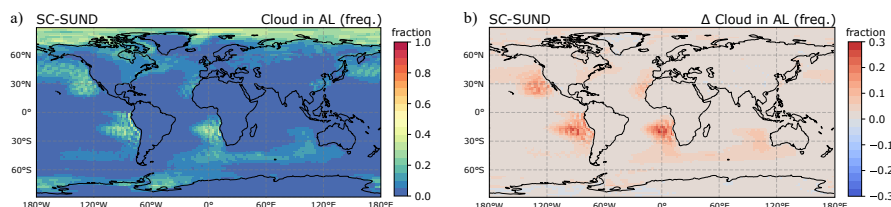
**Figure 9.** Presence of a cloud in the ambiguous layer in the SC-SUND simulation: (a) frequency (cf. Fig. 7c), (b) frequency increase compared to before application of SC-SUND.

The total cloud cover change experienced in the annual mean by the radiation routine in the SC-SUND simulation is quite large, reaching up to 15 pp in some columns and affecting extended areas (Fig. 6e). It is of comparable magnitude to that in

485 the SC-MAX simulation (Fig. 6g). However, it is interesting to note that the effect that is then produced on the simulated total cloud cover is much less marked with SC-SUND than with SC-MAX (see Fig. 6f and 6h). The reason for this may be linked to the fact that the process by which the annual mean total cloud cover seen by the radiation routine is increased is different in the two set-ups. In SC-MAX, the annual mean increases because all simulated stratocumulus clouds become 100% covering, but their number remains the same. In SC-SUND, it increases because the scheme can form new clouds and hence stratocumulus

490 clouds appear more frequently, with their coverage being calculated as usual. Thus, in SC-MAX, sunlight is scattered back to space almost fully in all situations with a stratocumulus cloud, which can have a very drastic effect on the radiation balance in stratocumulus regions; on the other hand in SC-SUND the increase in shortwave scattering in stratocumulus regions is more evenly distributed over time and may hence produce a more moderate effect on the meteorological conditions in those regions. In addition, the effect produced in SC-SUND may be weaker because the new clouds occurring in the scheme, although they

495 have a more realistic cloud cover, are likely to have a too-low liquid or ice content. Their liquid or ice content comes from the condensation or deposition computed using the original grid's gridbox mean RH, i.e. at low supersaturation, or from transport - both resulting in low amounts. This is a disadvantage of SC-SUND, as to have realistic liquid or ice content the grid refinement should be applied in the cloud microphysics scheme too. The water content in the SC-MAX clouds is likely higher, as there RH was high enough to form cloud cover.

500 These results indicate that the cloud cover improvement obtained in the radiation routine thanks to the implementation of *invgrid* is 'lost', as the radiative impact is too weak for the changes to be propagated to the simulated climate, probably due to a too-low water content in the new clouds. Despite the higher complexity, it may be beneficial to implement the grid refinement scheme directly in the cloud-related microphysics and cover routines in order to obtain a sizeable improvement in ECHAM-HAM's simulated stratocumulus clouds.

**Table 4.** Global and regional averaged occurrence frequency in the SC-SUND simulation of having a cloud in the ambiguous layer, and of forming a new cloud in the ambiguous layer.

|  | Global | NAM | SAM | AFR | BAR |
|---|---|---|---|---|---|
| Cloud in AL after SC-SUND (%) | 4.1 | 9.9 | 10.8 | 13.3 | 12.2 |
| New cloud formed in AL (%) | 1.8 | 7.1 | 7.9 | 10.2 | 1.9 |

## 4   Summary and conclusions

Two parametrisations for stratocumulus cloud cover based on a vertical grid refinement at the level of the capping inversion were developed and implemented only in the radiation routine of the ECHAM-HAM GCM. SC-VOLUME uses a geometrical and physical argument to augment the cloud's horizontal extent under the inversion; SC-SUND makes use of the improved temperature and water profile at the inversion and re-evaluates the cloud cover.

The inclusion of SC-VOLUME did not lead to significant improvements for the model's cloud cover bias in long-term global climate simulations. Some limitations of the method were highlighted. Firstly, the simulated stratocumulus clouds are very rarely occurring in the model layer containing the inversion and appear instead more often in an underlying layer, revealing a bias in the model's representation which may be due to a poor resolution of the humidity profile. As the correspondence of inversion layer and cloud layer is a necessary condition for the application of SC-VOLUME's cloud constraining method, this means that the scheme can only be applied in a small fraction of the identified stratocumulus cloud cases, limiting its general effect. Having identified this common stratocumulus-inversion layer mismatch is valuable, as it explains why a geometry-based method for the representation of stratocumulus clouds such as SC-VOLUME is not widely applicable and suggests that it would work better with a higher vertical resolution - which would improve stratocumulus cover representation regardless. Secondly, even in cases in which it is applied, SC-VOLUME tends to produce only a relatively small increase in the layer's cloud cover. With the SC-MAX experiment we showed that the model's stratocumulus cover bias is not only due to an underestimation of simulated clouds' horizontal extent, but also to an underestimation of their occurrence frequency and the areas where they appear. Hence, we conclude that a method like SC-VOLUME, addressing only pre-existing clouds, is too limited.

The SC-SUND scheme aimed to address both of the issues limiting SC-VOLUME. In fact, its application led to the formation of new clouds in the refined below-inversion grid layers and hence to a larger increase of the total cloud cover seen by the radiation routine compared to SC-VOLUME. Through some feedbacks this positive effect is perceived also by the simulated cloud cover, which increased and slightly reduced the bias to observations - however, this effect remains minor compared to the bias's magnitude. Changes to stratocumulus cloud representation, if applied in the radiation routine only, are hardly passed on to the model's general representation. Therefore, despite its numerical advantages, the implementation of a stratocumulus cloud parametrisation limited to the radiation routine is mostly unprofitable.

As the developed grid refinement method itself works well and improves stratocumulus cloud cover within the radiation routine, where it is currently applied, it could be valuable in the future to expand its use to other parts of the model as well.

As a further step, the grid refinement could be applied in the cloud microphysics routine, where an improved method for the reconstruction of the water content profile around the inversion could be developed, and in the cloud cover routine. This integration would allow it to have an effect on the calculation of cloud-related processes and directly improve the representation

535  of the simulated stratocumulus clouds in the model.

*Code and data availability.*  The ECHAM-HAMMOZ model is made freely available to the scientific community under the HAMMOZ Software License Agreement, which defines the conditions under which the model can be used. More information can be found at the HAMMOZ website (https://redmine.hammoz.ethz.ch/projects/hammoz, last access: 21 September 2020). The data used to produce the figures in this manuscript can be found at https://doi.org/10.5281/zenodo.4268194; scripts can be found at https://doi.org/10.5281/zenodo.4268168. The

540  Calipso-GOCCP product can be obtained from http://climserv.ipsl.polytechnique.fr/cfmip-obs/. The EPIC campaign data can be obtained from https://atmos.washington.edu/~breth/EPIC/EPIC2001_Sc_ID/sc_integ_data_fr.htm (Bretherton, 2005). The observational climatology of cloud occurrence frequency can be obtained from https://atmos.uw.edu/CloudMap/ (Hahn and Warren, 2007; Eastman et al., 2014).

*Author contributions.*  DN conceived the idea for the study. PP designed the experiments with help from DN and UL. PP implemented the vertical grid refinement schemes and conducted the simulations. PP analysed the results with contributions from DN and UL. PP wrote the

545  paper with comments from DN and UL.

*Competing interests.*  The authors declare that they have no conflict of interest.

*Acknowledgements.*  The ECHAM-HAMMOZ model is developed by a consortium composed of ETH Zurich, Max Planck Institut für Meteorologie, Forschungszentrum Jülich, University of Oxford, the Finnish Meteorological Institute and the Leibniz Institute for Tropospheric Research, and managed by the Center for Climate Systems Modeling (C2SM) at ETH Zurich. We would like to thank Colombe Siegenthaler-

550  Le Drian for her previous work in the model and for the helpful discussions.

# References

Boucher, O., Randall, D., Artaxo, P., et al.: Clouds and aerosols, chap. 7, Cambridge University Press, 2013.

Boutle, I. A. and Morcrette, C. J.: Parametrization of area cloud fraction, Atmospheric Science Letters, 11, 283–289, https://doi.org/10.1002/asl.293, https://rmets.onlinelibrary.wiley.com/doi/abs/10.1002/asl.293, 2010.

555 Bretherton, C. S.: EPIC Stratocumulus Integrated Dataset, https://atmos.washington.edu/~breth/EPIC/EPIC2001_Sc_ID/sc_integ_data_fr.htm, [Accessed December 2019], 2005.

Bretherton, C. S., Uttal, T., Fairall, C. W., Yuter, S. E., Weller, R. A., Baumgardner, D., Comstock, K., Wood, R., and Raga, G. B.: The Epic 2001 Stratocumulus Study, Bulletin of the American Meteorological Society, 85, 967–978, https://doi.org/10.1175/bams-85-7-967, 2004.

Caldwell, P., Bretherton, C. S., and Wood, R.: Mixed-Layer Budget Analysis of the Diurnal Cycle of Entrainment in Southeast Pacific
560 Stratocumulus, Journal of the Atmospheric Sciences, 62, 3775–3791, https://doi.org/10.1175/jas3561.1, 2005.

Chepfer, H., Bony, S., Winker, D., Cesana, G., Dufresne, J. L., Minnis, P., Stubenrauch, C. J., and Zeng, S.: The GCM-Oriented CALIPSO Cloud Product (CALIPSO-GOCCP), Journal of Geophysical Research, 115, https://doi.org/10.1029/2009jd012251, 2010.

Dietlicher, R., Neubauer, D., and Lohmann, U.: Prognostic parameterization of cloud ice with a single category in the aerosol-climate model ECHAM(v6.3.0)-HAM(v2.3), Geoscientific Model Development, 11, 1557–1576, https://doi.org/10.5194/gmd-11-1557-2018, 2018.

565 Eastman, R., Warren, S. G., and Hahn, C. J.: Climatic Atlas of Clouds over Land and Ocean, https://atmos.uw.edu/CloudMap/WebO/index.html, 2014.

Grenier, H. and Bretherton, C. S.: A Moist PBL Parameterization for Large-Scale Models and Its Application to Subtropical Cloud-Topped Marine Boundary Layers, Monthly Weather Review, 129, 357–377, https://doi.org/10.1175/1520-0493(2001)129<0357:amppfl>2.0.co;2, 2001.

570 Hahn, C. and Warren, S.: A Gridded Climatology of Clouds over Land (1971-96) and Ocean (1954-97) from Surface Observations Worldwide, Carbon Dioxide Information Analysis Center (CDIAC) Datasets, https://doi.org/10.3334/cdiac/cli.ndp026e, 2007.

Klein, S. A. and Hartmann, D. L.: The Seasonal Cycle of Low Stratiform Clouds, Journal of Climate, 6, 1587–1606, https://doi.org/10.1175/1520-0442(1993)006<1587:tscols>2.0.co;2, 1993.

Lenderink, G. and Holtslag, A. A. M.: Evaluation of the Kinetic Energy Approach for Modeling Turbulent Fluxesin Stratocumu-
575 lus, Monthly Weather Review, 128, 244–258, https://doi.org/10.1175/1520-0493(2000)128<0244:EOTKEA>2.0.CO;2, https://doi.org/10.1175/1520-0493(2000)128<0244:EOTKEA>2.0.CO;2, 2000.

Mauritsen, T., Bader, J., Becker, T., Behrens, J., Bittner, M., Brokopf, R., Brovkin, V., Claussen, M., Crueger, T., Esch, M., Fast, I., Fiedler, S., Fläschner, D., Gayler, V., Giorgetta, M., Goll, D. S., Haak, H., Hagemann, S., Hedemann, C., Hohenegger, C., Ilyina, T., Jahns, T., Jimenéz-de-la Cuesta, D., Jungclaus, J., Kleinen, T., Kloster, S., Kracher, D., Kinne, S., Kleberg, D., Lasslop, G., Kornblueh, L.,
580 Marotzke, J., Matei, D., Meraner, K., Mikolajewicz, U., Modali, K., Möbis, B., Müller, W. A., Nabel, J. E. M. S., Nam, C. C. W., Notz, D., Nyawira, S.-S., Paulsen, H., Peters, K., Pincus, R., Pohlmann, H., Pongratz, J., Popp, M., Raddatz, T. J., Rast, S., Redler, R., Reick, C. H., Rohrschneider, T., Schemann, V., Schmidt, H., Schnur, R., Schulzweida, U., Six, K. D., Stein, L., Stemmler, I., Stevens, B., von Storch, J.-S., Tian, F., Voigt, A., Vrese, P., Wieners, K.-H., Wilkenskjeld, S., Winkler, A., and Roeckner, E.: Developments in the MPI-M Earth System Model version 1.2 (MPI-ESM1.2) and Its Response to Increasing CO2, Journal of Advances in Modeling Earth Systems,
585 11, 998–1038, https://doi.org/10.1029/2018MS001400, https://agupubs.onlinelibrary.wiley.com/doi/abs/10.1029/2018MS001400, 2019.

Nam, C., Bony, S., Dufresne, J.-L., and Chepfer, H.: The 'too few, too bright' tropical low-cloud problem in CMIP5 models, Geophysical Research Letters, 39, https://doi.org/10.1029/2012gl053421, 2012.

Neubauer, D., Lohmann, U., Hoose, C., and Frontoso, M. G.: Impact of the representation of marine stratocumulus clouds on the anthropogenic aerosol effect, Atmospheric Chemistry and Physics, 14, 11 997–12 022, https://doi.org/10.5194/acp-14-11997-2014, https://www.atmos-chem-phys.net/14/11997/2014/, 2014.

590 PCMDI: AMIP Sea Surface Temperature and Sea Ice: Observational and Boundary Condition Data Sets, https://pcmdi.llnl.gov/mips/amip/, 2018.

Roach, W. T., Brown, R., Caughey, S. J., Crease, B. A., and Slingo, A.: A field study of nocturnal stratocumulus: I. Mean structure and budgets, Quarterly Journal of the Royal Meteorological Society, 108, 103–123, 1982.

595 Siegenthaler-Le Drian, C.: Stratocumulus clouds in ECHAM5-HAM, Ph.D. thesis, ETH Zürich, 2010.

Stevens, B., Moeng, C.-H., and Sullivan, P. P.: Large-Eddy Simulations of Radiatively Driven Convection: Sensitivities to the Representation of Small Scales, Journal of the Atmospheric Sciences, 56, 3963–3984, https://doi.org/10.1175/1520-0469(1999)056<3963:LESORD>2.0.CO;2, https://doi.org/10.1175/1520-0469(1999)056<3963:LESORD>2.0.CO;2, 1999.

Sundqvist, H., Berge, E., and Kristjánsson, J. E.: Condensation and Cloud Parameterization Studies with a Mesoscale Numerical Weather Prediction Model, Monthly Weather Review, 117, 1641–1657, https://doi.org/10.1175/1520-0493(1989)117<1641:cacpsw>2.0.co;2, 1989.

Tegen, I., Neubauer, D., Ferrachat, S., Siegenthaler-Le Drian, C., Bey, I., Schutgens, N., Stier, P., Watson-Parris, D., Stanelle, T., Schmidt, H., Rast, S., Kokkola, H., Schultz, M., Schroeder, S., Daskalakis, N., Barthel, S., Heinold, B., and Lohmann, U.: The global aerosol–climate model ECHAM6.3–HAM2.3 – Part 1: Aerosol evaluation, Geoscientific Model Development, 12, 1643–1677, https://doi.org/10.5194/gmd-12-1643-2019, https://www.geosci-model-dev.net/12/1643/2019/, 2019.

605 Wilks, D. S.: "The Stippling Shows Statistically Significant Grid Points": How Research Results are Routinely Overstated and Overinterpreted, and What to Do about It, Bulletin of the American Meteorological Society, 97, 2263–2273, https://doi.org/10.1175/BAMS-D-15-00267.1, https://doi.org/10.1175/BAMS-D-15-00267.1, 2017.

Wood, R.: Stratocumulus Clouds, Monthly Weather Review, 140, 2373–2423, https://doi.org/10.1175/mwr-d-11-00121.1, 2012.

Wood, R. and Bretherton, C. S.: On the Relationship between Stratiform Low Cloud Cover and Lower-Tropospheric Stability, Journal of
610 Climate, 19, 6425–6432, https://doi.org/10.1175/jcli3988.1, 2006.

Wood, R. and Hartmann, D. L.: Spatial Variability of Liquid Water Path in Marine Low Cloud: The Importance of Mesoscale Cellular Convection, Journal of Climate, 19, 1748–1764, https://doi.org/10.1175/jcli3702.1, 2006.

Yamaguchi, T., Feingold, G., and Larson, V. E.: Framework for improvement by vertical enhancement: A simple approach to improve representation of low and high-level clouds in large-scale models, Journal of Advances in Modeling Earth Systems, 9, 627–646,
615 https://doi.org/10.1002/2016MS000815, https://agupubs.onlinelibrary.wiley.com/doi/abs/10.1002/2016MS000815, 2017.